Effect of Silica Surface Properties on the Formation of Multilayer or Sub-monolayer Protein Hard Corona: Albumin Adsorption on Pyrolytic and Colloidal SiO2 Nanoparticles

UNIVERSITÀ DEGLI STUDI DI TORINO

J.Phys. Chem- C, **2015**, *119 (11),* pp 26493−26505,

DOI: 10.1021/acs.jpcc.5b07764

Effect of Silica Surface Properties on the Formation of Multilayer or Sub-monolayer Protein Hard Corona: Albumin Adsorption on Pyrolytic and Colloidal SiO_2 Nanoparticles

Federico Catalano,[#] Gabriele Alberto,[†,] Pavlo Ivanchenko,[†] Galyna Dovbeshko[‡] and Gianmario Martra[†,*]*

#Department of Clinical and Biological Sciences, Regione Gonzole 10, 10043 Orbassano (TO), Italy

†Department of Chemistry and Interdepartmental Nanostructured Interfaces and Surfaces (NIS) Centre, University of Torino, via P. Giuria 7, 10125 Torino, Italy;

[‡]Institute of Physics of the National Academy of Science of Ukraine, 46 Nauki Ave., Kyiv 03028, Ukraine.

Keywords: Silica nanoparticles, surface silanols, BSA, protein corona, particle agglomeration.

ABSTRACT

The adsorption of bovine serum albumin (BSA) on two types of silica nanoparticles (NPs), one pyrolytic (P–SiO_2; namely AOX50 by Evonik) and the other colloidal (lab-made by using inverse micelles microemulsion, M–SiO_2), is studied. Both materials are characterized in terms of size of primary particles (by transmission electron microscopy), amounts (by thermogravimetry) and distribution of silanols (IR spectroscopy in controlled atmosphere, augmented by H/D isotopic exchange and reaction with $VOCl_3$, to distinguish silanols actually located at the surface of nanoparticles), water contact angle, ζ–potential and dispersion state in water, PBS buffer and BSA solutions in PBS (by dynamic light scattering, DLS). Proteins are found to act as dispersing agent toward the large aggregates formed by both types of NPs in PBS buffer, although monodispersion was not attained in the conditions investigated. The problem of the determination of the silica surface actually available in NPs agglomerates for protein adsorption is addressed, and a model based on the external area of the agglomerates determined by DLS is proposed, supported by the trend of ζ–potential in dependence on the amount of adsorbed BSA and by the UV circular dichroism spectra of adsorbed proteins. The spectra reveal the occurrence of protein-protein interactions for BSA on P–SiO_2, where multilayers of irreversibly adsorbed BSA molecules (i.e. a so called protein hard corona) are proposed to be formed. Conversely, the model indicates the formation of a sub-monolayer protein hard corona on M–SiO_2. The difference in protein coverage appears to be related to differences in the distribution of surface silanols, more than to differences in ζ–potential.

INTRODUCTION

Silica and silica-based materials can have noxious or beneficial effect, and their interaction with the human body has been investigated for a long time. In the case of noxious effects, the reason for the interest has been to uncover useful structure-activity relationships to explain the well-documented toxicity of crystalline silica particles.[1] In the case of beneficial effects, a typical example is Hench bioglasses.[2] More recently, this scenario has been enriched by actual or potential uses of silica nanoparticles (NPs) in nanomedicine, beginning with seminal research works carried out in the in the first decade of the 20th century, dealing with the use of SiO_2 as drug-delivery system,[3] or as the basis for the fabrication of engineered multifunctional systems.[4] In general, the SiO_2 NPs in the huge amount of subsequent investigations in the fields of nanomedicine and nanobiotechnology can be classified into two main categories: porous (typically mesoporous)[5-7] and nonporous.[8] The possibility of forming a silica shell on different types of cores (e.g., gold, quantum dots, iron oxides) can also be exploited for the preparation of composite NPs.[4]

Independently of the NP type, the fields of nanomedicine and nanobiotechnology are well aware that the interaction of NPs with a biological medium, both *in-vitro* and *in-vivo*, is mediated by the so called "protein corona" resulting from protein molecules present in the incubation media or biofluids adsorbing in the NP surfaces.[9-11] The importance of protein-adsorbed biointerfaces has been recognized for implanted biomaterials, as a step in the causal sequence (i) biomaterial surface structure, (ii) states of adsorbed water molecules, and (iii) states of adsorbed proteins, ruling the fate of the interaction of the implant with cells.[12] Moreover, the protein corona has recently been reported as an in-situ biosensor for temporal and local biomarkers in

tissue-engineered scaffolds.[13]

The quantitative, compositional, and structural features of a protein corona formed on NPs in cell culture media are the result of a multi-parameter process involving rich salt and protein compositions, adsorption–desorption energetics and dynamics of proteins (often determining a significantly different corona composition with respect to the incubation medium), and the surface characteristics of NPs.[10]

Although such complex systems are the targets of primary interest, another direction in investigations of the protein corona is the study of model systems where NPs are in contact with only one type of protein molecule. This allows for more quantitative investigations involving possible conformational changes of adsorbed proteins. In this respect, bovine serum albumin (BSA) is widely used as a model/probe molecule to study protein adsorption on SiO_2,[14,15] Al_2O_3,[16] Ag,[17] and CeO_2[18] NPs, because of the huge amount of available data on the structural features of this protein, the high degree of homology with respect to human serum albumin,[19] and its low cost.

Protein adsorption on solid surfaces remains "a common but very complicated phenomenon," as stated by Nakanishi et al.[20] To date, many studies have been carried out in this field, and significant advances have been attained in regard to the three main factors for controlling the adsorption of a single protein species: external parameters (temperature, pH, ionic strength, buffer/media composition), protein properties, and surface properties.[21] For the surface properties in particular, the adsorption of proteins on SiO_2 NPs was investigated in regard to its dependence on the size and surface curvature,[22-24] surface functionalization with poly(ethylene glycol),[24] amino[25,26] or carboxylic[26] groups, and amount of surface silanols, changed by tuning

the flame pyrolysis conditions,[27] or post-synthesis firing at high temperature[28]or hydrothermal treatments.[29]

The relative amount and distribution of these sites with respect to siloxane bridges (the other type of linkage exposed by silica particles) rule relevant aspects of the physical-chemical behavior of the silica surface towards both water, determining the hydrophobic/hydrophilic character,[30] and proteins.[28,29] Of course, when different types of silica NPs are considered, a source of differences in the surface silanol populations is the preparation method of the material, which can basically be associated with one of the two following processes: i) flame pyrolysis of $SiCl_4$, producing the so-called fumed silicas, or ii) condensation in aqueous media of ≡Si–OH moieties, forming ≡Si–O–Si≡ linkages. This aspect has recently been considered in a study on the dependence of silica NP toxicity on the production process by comparing fumed and colloidal silicas.[31]

Colloidal silicas are among the SiO_2 NPs resulting from type ii) processes and are typically nonporous spherical NPs produced by hydrolysis (followed by condensation) of Si alkoxydes in homogeneous or heterogeneous systems. The first condition is typical of the well-known "Stöber method,"[32] while in the second case, hydrolysis occurs in inverse micelles formed in water in oil reverse microemulsions.[33] Nonporous SiO_2 NPs produced by both of these methods are of interest for biomedical uses. Applications range from the delivery of conjugated or encapsulated small drugs, proteins, genes, or agents active in photodynamic therapy to molecular imaging by incorporation of contrast agents or photoluminescent dyes.[8]

Interestingly, colloidal silica NPs were found to exhibit a mass fractal structure[31] that effectively accounts for the huge content in silanol groups, most of which are located below the

external surface of NPs.[35] When studying the interaction of these NPs with proteins, an additional task remains in the recognition of silanols that are actually exposed at the external surface. We carried out a comparative study of BSA adsorption on pyrogenic and microemulsion-based silica NPs (hereafter referred to as P–SiO_2 and M–SiO_2, respectively). Several features of the materials were measured and investigated, like the size and morphology (by transmission electron microscopy), relative distribution of surface silanols (by IR spectroscopy in controlled atmosphere augmented by isotopic H/D exchange and a new method to recognize surface ≡Si–OH among the overall silanols content of M–SiO_2), ζ-potential, dispersion state in buffer suspension, and the dependence on the BSA concentration in the incubation media (by dynamic light scattering). Particular attention has been devoted to the calculation of the surface coverage by proteins and the dependence on the agglomeration of NPs, which is supported by the use of UV circular dichroism for monitoring the occurrence of protein–protein interactions expected in the presence of multilayered BSA protein corona. In this respect, this work would contribute to emerging need of quantitative studies to further the understanding of protein corona formation.[36]

EXPERIMENTAL SECTION

Materials All solvents and reagents [ethanol, acetone, tetraethylorthosilicate, aminopropyltriethoxysilane, cyclohexane, n-hexanol, Triton X-100, ammonia, BSA, phosphate buffer saline PBS, deuterated water (99.9 atom % D), n-heptane and anhydrous vanadium (III) chloride] were high-purity Sigma-Aldrich products and used as received. Pyrolytic silica

Aerosil® OX 50 (P–SiO_2) was purchased from Evonik. MilliQ water was used throughout.

Synthesis and Lab-made Silica NPs. Microemulsion-based silica NPs (M–SiO_2) were prepared by the following the procedure.[37,38] Briefly, a microemulsion was prepared by mixing cyclohexane (150 mL), *n*-hexanol (36 mL), Triton X-100 (35.4 mL), and deionized water (10.8 mL). The mixture was gently stirred for 30 minutes at room temperature (r.t.) to reach homogeneity. Then, tetraethylorthosilicate (TEOS, 9 mmol, 2 mL) and NH_4OH (28-30%, 5.3 mmol; 0.7 mL) were added to the microemulsion to start the reaction. The mixture was stirred for a further 16 hours at r.t., and the reaction was then interrupted by the addiction of acetone (100 mL). NPs were extracted from the reaction mixture by centrifugation (10000 rpm, 20 min, r.t.) and then washed twice with absolute ethanol and several times with deionized water to completely remove surfactant molecules. The obtained sample was then stored in aqueous suspension.

Transmission Electron Microscopy (TEM). TEM images were obtained with a 3010 Jeol instrument operated at 300 kV. Samples were prepared by spreading a droplet of the suspended particles on a copper grid coated with a lacey carbon film. The liquid was then allowed to slowly evaporate to limit the aggregation of NPs. For the histogram of the NP size distribution, the diameters of ca. 300 particles were measured, and the mean value was calculated as $d_m=\sum d_i n_i/\sum n_i$, where n_i is the number of particles of diameter d_i. The results are expressed as $d_m \pm$stdv.

Specific Surface Area (SSA_{BET}) Measurements. Specific surface areas of both P– and M–SiO_2 were measured by N_2 adsorption–desorption isotherms at 77 K using a Micromeritics ASAP

2020 instrument. The SSA was calculated by the Brunauer–Emmett–Teller (BET) method.

Thermogravimetric Analysis (TGA). TGA measurements were carried out on the silica samples in powder form (TA Instruments SDT Q600). Samples were dried at r.t. in a vacuum oven, and then 10-mg aliquots were placed in the sample holder. TGA measurements were performed under a constant air flux (0.1 $L \cdot min^{-1}$) with a heating rate of 10 $K \cdot min^{-1}$ from r.t. to 1273 K.

IR Measurements. M–SiO_2 and P–SiO_2 powders were pressed in self-supporting pellets with "optical thickness" of ca. 10–15 $mg \cdot cm^{-2}$. The samples were then inserted in a cell equipped with CaF_2 windows and attached to a conventional vacuum line (residual pressure $\leq 5 \cdot 10^{-5}$ mbar) in order to carry out adsorption/desorption experiments in situ. Spectra were collected with a Bruker IFS28 spectrometer (resolution 4 cm^{-1}; MCT detector) by accumulating 150 scans to obtain a good signal-to-noise ratio. The spectra were reported in absorbance after scattering correction. All spectra were also normalized with respect to the intensity of signals at 1980 and 1870 cm^{-1} due to combinations of silica bulk framework modes.[39] This was done to render differences in intensity, independent of different thicknesses among pellets.

Spectra were collected at beam temperature (b.t.; ca. 323 K) in air and after outgassing to remove water molecules adsorbed on the surface. In separate experiments, D_2O and $VOCl_3$ were applied to the outgassed samples after several freeze-pump-thaw cycles. D_2O adsorption and desorption cycles were repeated until no changes occurred in the spectra.

Dynamic Light Scattering (DLS). DLS measurements were performed in a 90Plus Particle Size Analyzer (Brookhaven Instruments) at a laser wavelength of 660 nm, a detection angle of 90°, and 293 K. Samples were prepared by suspending NPs in MilliQ water (pH 5.5) and PBS (pH

7.4). The NPs agglomeration was also investigated when suspended in the BSA solution and in the presence of only the irreversibly adsorbed proteins in separate experiments (see "Adsorption of BSA on silica samples" section for the detailed procedure). In all cases, the NP concentration was 0.1 $mg \cdot mL^{-1}$. DLS plots are reported in mass distribution from the results of triplicate experiments. Raw data for bare particles, BSA in PBS, and suspensions of NPs with adsorbed proteins are reported in both mass and number distribution in Figure S1 in the supporting information (SI hereafter).

ζ-potential. The surface potential of bare silica NPs suspended in MilliQ water and PBS and that of NPs carrying irreversible adsorbed BSA and suspended in PBS (see "Adsorption of BSA on silica samples" section for the procedure) were measured by electrophoretic light scattering (ELS) using a Zetasizer Nano-ZS (Malvern Instruments). Data are reported as means values of triplicate experiments.

Contact Angle Measurements. The Washburn capillary rise method was applied to measure the water contact angle of the silica NPs. A dynamic contact angle was measured with Krüss 100K tensiometer. The Washburn tube (6 cm long, 11 mm inner diameter), were particles were sieved and compacted, was placed into close contact with water, and the weight of the water penetrated into the packed bed was recorded as a function of time. By plotting the weight square values (m^2) versus time (t), the water contact angle (θ) was calculated according the Washburn equation:

$$\frac{m^2}{t} = c\,\frac{\rho^2 \gamma_l \cos\vartheta}{\mu} \qquad (1)$$

where $m^2\ t^{-1}$ is the uptake rate of $mass^2$ as liquid rises into particle bed, c is the capillary

constant typical of the material packing geometric, ρ is the liquid density, γ_l is the surface tension of the liquid, θ is the particle-liquid contact angle and μ the liquid viscosity.[40] The capillary constant for both materials was appointed by calibration runs with an ideal wetting liquid (n-heptane, density = 0.68 $g \cdot mL^{-1}$, surface tension = 19.39 10^{-3} $N \cdot m^{-1}$ and viscosity = 0.41 10^{-3} $Pa \cdot s$). Afterwards, the measurements were carried out with MilliQ water and PBS as wetting fluids. The reported water contact angle value of each material is the average of three measurements. The particle wetting curves (m^2 vs t) are displayed in Figure S2 in the SI.

Adsorption of BSA on Silica Samples. For all samples, a series of 50-mg suspensions of NPs in 2.5 mL of PBS was prepared and sonicated for 15 min at 298 K. Different incubation solutions were prepared by adding different amounts of BSA to 2.5 mL of PBS. Each BSA in PBS solution was then added to one of the 2.5-mL suspensions of silica NPs in PBS. The nominal concentrations of BSA in the final volumes (5.0 mL) were 0.1, 0.5, 1.0, 2.5, 5, and 7.5 $mg \cdot mL^{-1}$. The samples were placed in centrifuge tubes and rotated end-over-end for 15 min at 298 K (longer incubation times did not result in significant differences in the amount of adsorbed BSA; data not shown). Powders were then separated from the incubation medium by centrifugation (10000 rpm, 20 minutes, 298 K), and the supernatants were removed. Pellets with adsorbed BSA underwent several re-suspension/centrifugation cycles with fresh PBS to desorb proteins reversibly adsorbed toward dilution. Finally, each sample was resuspended in 5.0 mL of PBS for spectrophotometric analyses (vide infra).

Quantification of Adsorbed BSA. The usual method was used for determining the amount of proteins in an aqueous solution by spectroscopic measurement of the absorbance at λ = 280 nm (Cary 300 Bio, Varian). A calibration curve (absorbance λ = 280 nm vs. BSA concentration in

mol·L^{-1}) was established, including the BSA concentrations of the incubation solutions. After incubation, the supernatant obtained from the first centrifugation was separated from the powder, subjected to two subsequent additional centrifugations, and analyzed spectrophotometrically at λ = 280 nm. The basis for determining the total amount of adsorbed BSA (reversibly + irreversibly) was the difference between the initial concentration of BSA in the incubation solutions (determined as indicated in the previous section) and the BSA concentration in the corresponding supernatants.

The slurries resulting from the first centrifugation were then re-suspended/centrifuged 3 times each in 2 mL of fresh PBS. For each slurry, the supernatants resulting from washing were merged and analyzed spectrophotometrically to determine the BSA content corresponding to the amount of reversibly adsorbed proteins. Then, the difference between the total amount of adsorbed proteins and the amount of those desorbed by washing with protein-free PBS resulted in the amount of irreversibly adsorbed BSA molecules. Hence, in this work the terms "irreversibly adsorbed proteins" will be referred to the irreversibility toward dilution of proteins in the suspension medium. Results are reported as the mean value of at least three separate experiments ± stdv.

Circular Dichroism Spectroscopy (CD-UV). Solutions of 0.1-mg·mL^{-1} BSA, both as received and thermally treated (374 K, 15 min), were scanned in the far-UV spectral range (four accumulations) over the wavelength region of 180-300 nm with a scanning speed of 50 nm·min^{-1}. This was done using a Jasco J-815 spectropolarimeter equipped with a Xe arc lamp and a quartz circular cuvette (path length 0.1 cm). MilliQ water was used as a solvent because PBS is not transparent in the range of 180–200 nm. For analyses of BSA irreversibly adsorbed on silica

NPs, the samples that were separated from the incubation medium as indicated above were suspended in MilliQ water just before acquiring spectra. The amount of silica NPs in the suspension was then diluted to minimize scattering due to particle suspension (1.0–0.5 $mg \cdot mL^{-1}$). Based on the amount of adsorbed proteins per mass unit of NPs (see previous section), the BSA concentration in each suspension was then determined and adjusted to obtain the same nominal concentration of irreversibly adsorbed BSA in units per volume of sample (see comments of Figure S4 in the SI). Resulting CD spectra, were then deconvoluted using CDNN deconvolution software (Version 2.1, Copyright (C) 1997 Gerald Böhm) for the secondary structure estimation. CDNN software works with a neural network, an artificial intelligence program used to find correlation with reference database spectra. Parameters as molecular mass (Da), protein concentration ($mg \cdot mL^{-1}$), number of aminoacids and cuvette pathlength (cm) were use as input to upload CD files, expressed in mdeg in the 180-260 nm range. The deconvolution has been made considering the maximum number (33) of reference spectra in the database. Only results not exceeding the 100% of total sum of secondary structure and the 5% of standard deviation were considered as reliable in the 185-260 nm range. The reliability of deconvolution results was confirmed by the agreement with literature data of native and thermally treated BSA.

RESULTS AND DISCUSSION

Morphology and Size of Silica NPs. Figure 1 shows representative TEM images and the correspondent size distribution of P–SiO_2 and M–SiO_2 (Figure 1A,B and Figure 1C,D, respectively).

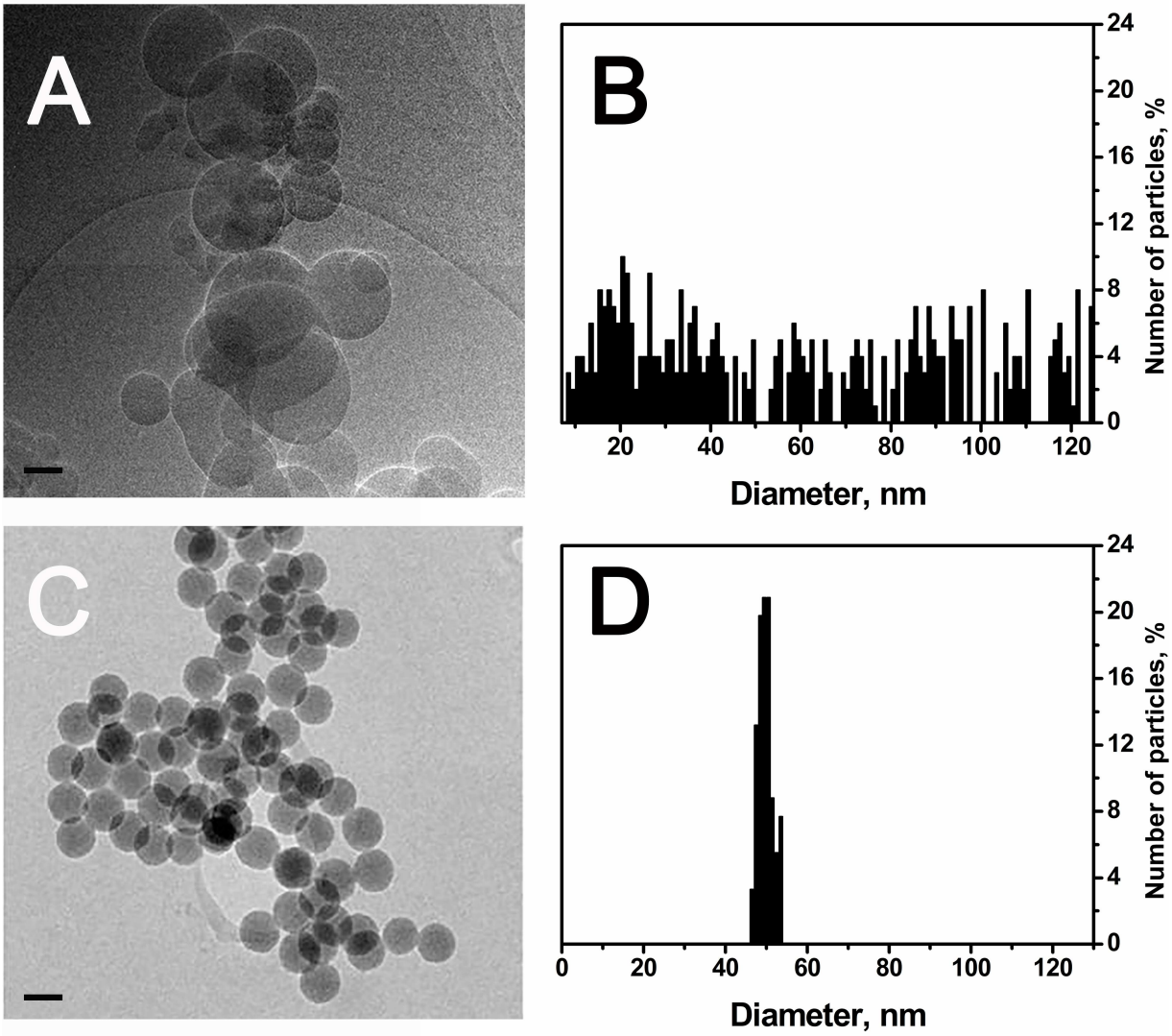

Figure 1. TEM images (A,C) and size distribution (B,D) of P–SiO_2 and M–SiO_2, upper and bottom panels, respectively. Scale bar = 50 nm.

The P–SiO_2 powder was made of roundish particles with highly heterogeneous shape and size and diameters distributed in the range of 10–120 nm. Conversely, M–SiO_2 appeared as spherical NPs with homogenous shape and size and a narrow size distribution centered at ca. 50 ± 2 nm. The different morphological features resulted in different specific surface areas with SSA_{BET} measurements providing values of ca. 50 $m^2 \cdot g^{-1}$ for P–SiO_2, which is in good agreement with

technical data provided by the supplier (50 ±15 $m^2 \cdot g^{-1}$). The measured value was 95 $m^2 \cdot g^{-1}$ for M–SiO_2 (Table1).

Table 1. Surface features of P–SiO_2 and M–SiO_2: specific surface area measured by N_2 adsorption isotherm (BET method) and number of silanols per nm^2 obtained by combining the results of thermogravimetric analyses with SSA_{BET} measurements.

sample	*specific surface area ($m^2 \cdot g^{-1}$)*	*silanols per nm^2*
P–SiO_2	50	1.6
M–SiO_2	95	30

Surface Silanols. The amount of silanols present in the two types of silica NPs was measured by TGA, and their average surface density was determined using the values of SSA_{BET} (Table 1, last column). A value of 1.6 Si–OH per nm^2 was found for P–SiO_2, whereas the density resulted in 30 silanols per nm^2 for M–SiO_2. Of course, such a value cannot be related only to silanols exposed on the surface of M–SiO_2 NPs measured by N_2 adsorption because the maximum amount of OH groups that can be present on the silica surface is 7 OH per nm^2.[41] Also, the density of silanols at the surface of P–SiO_2 was overestimated because of the presence of intraglobular ≡Si–OH (vide infra). To distinguish between surface and sub-surface silanols, SiO_2 NPs were placed in contact with D_2O, which was expected to produce a Si–OH/Si–OD isotopic exchange for only silanols accessible to vapor molecules. The process was monitored by in situ IR spectroscopy, and the results are summarized in Figure 2.

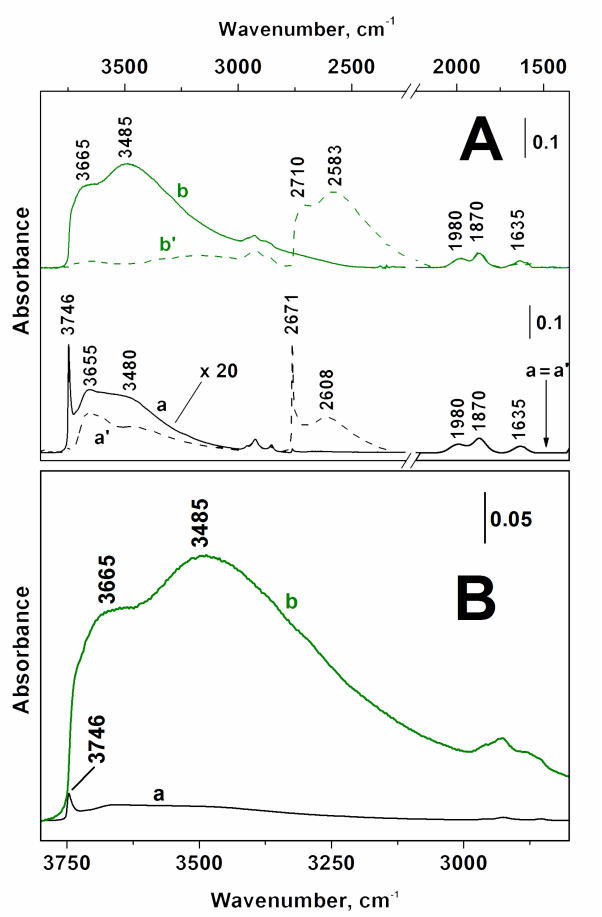

Figure 2. Panel A: IR spectra of P–SiO_2 (black curves) and M–SiO_2 (green curves) outgassed at r.t. (a, b, solid lines), and after H/D exchange by contact with D_2O and subsequent outgassing at r.t., repeated in sequence until invariance of spectra (a', b', dashed lines). Panel B: zoom of the νOH spectral region for P–SiO_2 (a, this time without multiplication for any extra factor) and M–SiO_2 (b) outgassed at r.t. In both panels the intensities were normalized with respect the 2000-1550 cm^{-1} pattern due to bulk modes (see Experimental section). In addition, curves a,a' in panel A were multiplied by 20, for the sake of clarity.

For P–SiO_2, the infrared profile of the NPs outgassed at r.t. exhibited a typical pattern with two groups of signals in the ranges of 3800-3000 cm^{-1} and 2000-1550 cm^{-1} (curve a). Based on

established literature data,[53,59] the pattern can be assigned to OH stretching (νOH) as follows:

- narrow peak at 3746 cm^{-1}: isolated silanols

- 3700-3600 cm^{-1}: Si–OH interacting via van der Waals/weak H-bonding (including intraglobular silanols)

- 3600-3000 cm^{-1}, broad features with partly resolved maximum at 3480 cm^{-1}: Si–OH interacting via H-bonding

- 1980 and 1870 cm^{-1} combinations of symmetric and antisymmetric bulk modes

- 1635 cm^{-1} overtone of symmetric bulk modes

The contact with D_2O (curve a') did not change the features in the low frequency region, confirming the complete desorption of H_2O molecules by outgassing at r.t., which, if otherwise present, should produce a δH_2O mode component at ca. 1640 cm^{-1} that would be expected to disappear after isotopic exchange. In contrast, the νOH pattern appears widely affected by the isotopic exchange, resulting in the disappearance of the νOH at 3746 and 3480 cm^{-1}, which was converted to νOD signals at 2761 cm^{-1} and 2608 cm^{-1}. This appears to be due to accessibility of silanols to D_2O molecules. In the νOH region, components at 3655 and 3450 cm^{-1} resisted the H/D exchange, indicating the presence of silanols located in intraglobular voids that are inaccessible to gaseous molecules, as known for pyrogenic silicas.[39]

For M–SiO_2, the νOH pattern after outgassing at b.t. (curve b) appeared to be dominated by a broad component with a maximum at 3475 cm^{-1}, which was accompanied on the high frequency side by a secondary maximum at 3765 cm^{-1} and an ill-resolved shoulder at 3730 cm^{-1}. This profile clearly indicates that these NPs contain a higher relative amount of silanols interacting

with each other via H-bonding. The νOH pattern was almost depleted by subsequent H/D exchange, which produced the corresponding OD pattern while leaving the signals at lower frequency unchanged, as in the previous case. The combination of the apparent surface density of silanols calculated based on the SSA_{BET} area (Table 1) and the sensitivity of almost all Si–OH in M–SiO_2 NPs to the H/D exchange leads to the conclusion that sub-surface silanols should be present, as mentioned above, but with sensitivity to the contact of NPs with D_2O. This behavior agrees well with what was observed for Stöber silica particles for which a mass fractal structure was proposed:[34] nitrogen molecules adsorbed at low temperature for measuring the SSA_{BET} cannot enter the H-bond network among silanols distributed from the surface towards the bulk of NPs, whereas this network can be entered by water molecules (also in the D_2O form) and/or by OH^- /H_3O^+ (OD^-/D_3O^+) species resulting from their auto dissociation. In fact, the contact of silica powders with the water vapor pressure at r.t. results in the surface formation of liquid-like H_2O/D_2O molecular multilayers where the auto dissociation of water molecules can occur.[42]

The presence of subsurface silanols in M–SiO_2 hindered the possibility of direct recognition of the Si–OH actually exposed on the surface of these NPs. The comparison between the normalized νOH profiles of the two types of NPs (Figure 2B) indicated that surface isolated silanols, if present, should be a very minor fraction among Si–OH in M–SiO_2. The difference in the amount of silanols in the two types of NPs effectively accounts for the relevant difference in the integrated intensity of the two profiles (ca. 15 times).

The contribution of the surface silanols to the overall νOH pattern of M–SiO_2 was then determined by back-exchange of deuterated NPs with tert–butanol to assess the accessibility of silanols by molecules with a larger cross section. However, the silanols sensitive to the D/H back

exchange appeared to be ca. 60% of the total; i.e., ca. 18 per nm^2 (Figure S3 in the SI). This value still resulted in significantly higher Si–OH surface density than the maximum expected for silica (see above), indicating that the back-exchange should have also involved a fraction of subsurface silanols, likely by swelling of the subsurface layers by contact with the alcohol vapors and/or the occurrence of a proton-like transfer mechanism between alcohol molecules adsorbed on the NP surfaces and the inner network of interacting silanols.

Both types of silica NPs were then placed in contact with $VOCl_3$, which reacts with Si-OH to produce grafted vanadyl species.[43,44]

$$3(\equiv\text{Si-OH}) + VOCl_3 \rightarrow [(\equiv\text{Si-OH})_{3-n}, (\equiv\text{Si-O})_n]VO(Cl)_{3-n} + n\ HCl \quad \text{with } 3 \geq n \geq 1$$

Because of the significant steric hindrance of the three Cl atoms and the need for actual contact between the reactants for the occurrence of the process, this reaction appeared to be a good candidate for the selective consumption of surface silanols in the case of $M–SiO_2$ as well. The reaction was monitored by in situ IR spectroscopy, and the results obtained for both types of silica NPs are displayed in Figure 3.

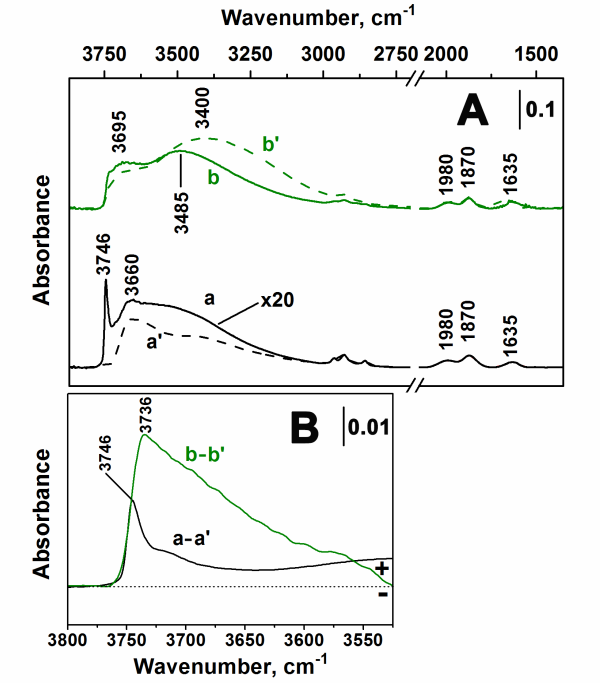

Figure 3. Panel A: IR spectra of P–SiO_2 (black curves) and M–SiO_2 (green curves) before (curves a,b, solid lines) and after (curves a',b', dashed lines) reaction with $VOCl_3$. The specra of the two materials were normalized with respect to the pattern in the 2000-1550 cm^{-1} range (see Experimental section). In addition, curves a,a' in panel A were multiplied by 20, for the sake of clarity. Panel B: results of the (a-a', this time without multiplication for any extra factor) and (b-b') spectra subtraction in the 3800-3500 cm^{-1} range. The intensities of the curves were normalized with respect to both the pattern in the 2000-1550 cm^{-1} range and the SSA_{BET}.

In the case of P–SiO_2 (Figure 3A, a,a'), the contact with $VOCl_3$ resulted in depletion of the νOH components due to the surface silanols, leaving a spectral pattern almost corresponding to the profile due to intra-globular ≡Si-OH previously revealed by H/D isotopic exchange (Figure 2, a'). It can be inferred that all surface ≡Si-OH was consumed in the grafting of vanadyl species,

likely producing only $(\equiv Si\text{-}O)_3VO$ species. In contrast, the admission of $VOCl_3$ on M–SiO_2 produced only a limited consumption of the νOH components above ca. 3500 cm^{-1}, accompanied by increased intensity of a broad feature in the range of 3500–3000 cm^{-1} (Figure 3A, b,b'). This should result from the H-bond interaction between unreacted Si-OH and Cl atoms of grafted vanadyl chloride species, indicating that $[(\equiv Si\text{-}OH)_{3-n}, (\equiv Si\text{-}O)_n]VO(Cl)_{3-n}$ species ($2 \geq n \geq 1$) should also be present in this case.

The increase of the intensity below 3500 cm^{-1} prevented the possibility of obtaining any quantitative information on the involvement in the reaction of H-bonded silanols possibly present on the surface of M–SiO_2 NPs. However, the subtraction between the spectra collected before and after the contact with $VOCl_3$ allowed for extracting of the profile due to surface silanols contributing to the spectral range above 3500 cm^{-1}. This analysis was carried out for both types of SiO_2 NPs, and the results are compared in Figure 3B. In the case of P–SiO_2 NPs, this spectral range is dominated by a peak at 3746 cm^{-1} due to isolated silanols (curve a-a'), whereas for the M–SiO_2, this signal (if present) should be a minor sub-band of an absorption with maximum at 3736 cm^{-1} and broaden towards lower wavenumbers (curve b-b'). Such a profile indicates that the surface of M–SiO_2 NPs should expose significantly larger relative amounts of silanols that are close enough to each other to interact through weak H-bonding.[39]

After normalization with respect to both the sample amount and SSA_{BET} (which are the obtained signals related only to surface Si–OH), the integrated area of the b-b' curve obtained for M–SiO_2 was ca. 2.6 times larger than that for the a-a' curve obtained for P–SiO_2. The stronger the interaction involving hydroxy groups, the larger the νOH downshift and increase of the decadic absorption coefficient.[45] The coefficient was found to be ca. 10 times higher for H-

bonded ≡Si–OH characterized by νOH below 3600 cm^{-1}.[46] Based on these findings, it seems reasonable to propose that the amount of silanols (weakly interacting) responsible for the νOH pattern in the range of 3800-3600 cm^{-1} might be similar for P–SiO_2 and M–SiO_2, or even slightly lower for the second one.

Agglomeration vs. Dispersion of SiO_2-NPs in BSA Solutions.

The state of SiO_2 NPs was investigated in terms of hydrodynamic diameter (Dh) and ζ-potential for NPs suspended in water and in PBS buffer and then added in this form to PBS buffer with different BSA concentrations (Figure 4, panels A and B, respectively; raw DLS data in Figure S1 in the SI).

(the remaining part of the page was intentionally left blank for showing in the same page following Figure 4 and related caption)

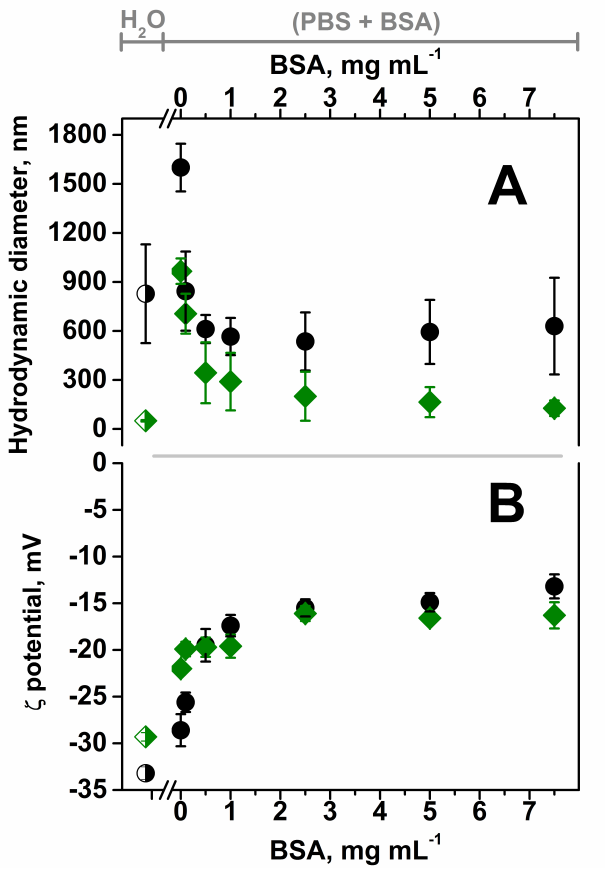

Figure 4. Hydrodynamic diameters (panel A) and ζ–potential values (panel B) of P–SiO_2 (black symbols) and M–SiO_2 (green symbols) suspended in PBS buffer (first full symbol), then added to BSA solutions with different protein concentrations, separated from the incubation media and then re-suspended in PBS buffer. Thus, data refers to the fraction of protein irreversibly adsorbed on particle agglomerates. For the sake of completeness, also data obtained by suspending bare P–SiO_2 and M–SiO_2 in MilliQ water are reported in the left part of both panels (half symbols, color code as in the rest of the figure).

Dh was measured both while keeping unadsorbed proteins in the suspension media and after removing them; i.e., leaving NPs with irreversibly adsorbed BSA molecules suspended in bare PBS buffer. Basically the same results were obtained for both cases (see Figure S1 in the SI). The second conditions were also used for the measurements of ζ-potential. Thus, for the sake of comparison, Figure 4A shows DLS data obtained for silica NPs with irreversibly adsorbed proteins. P–SiO_2 NPs (Figure 4A, black circles) suspended in MilliQ water exhibited an Dh of ca. 830 nm (half circle). This is distinctly larger than the particle size observed by TEM (Figure 1, panels A,B), indicating the occurrence of significant NP agglomeration. By considering that these particles exhibit a ζ-potential of −33 mV (see below), this behavior indicates that attractive hydrophobic forces and, as DLVO forces are concerned, attractive van der Waals forces prevailed in some extent on the electrostatic double layer repulsive force, actually entropic/osmotic in nature.[46] In this respect, a contact angle of 87.96 ± 0.24° was measured by P-SiO_2, close to the conventional boundary for a classification of a surface as hydrophobic (>90°) or hydrophilic (<90°).[48] This value is in agreement with the enthalpy of adsorption of water on P-SiO_2, found to be very close to the latent heat of water liquefaction,[30] considered as a reference threshold when measuring hydrophilicity/hydrophobicity by water adsorption calorimetry.[49] The addition of such agglomerates to PBS buffer resulted in a further increase of Dh to ca. 1600 nm, as a consequence of the decrease of the surface potential to −29 mV (see below) resulting from the presence of electrolytes in the buffer.[45] Conversely, the contact angle remained almost unchanged (88.47 ± 0.23°), as confirmed by the *t* test carried out at a 95% confidence level on the PBS and water measured contact angle values.

Then, aliquots of P–SiO_2 suspended in PBS buffer were added to buffered BSA solutions at different protein concentrations. DLS measurements revealed that the Dh of agglomerates sharply decreased to ca. 600 nm for BSA concentration as low as 0.5 $mg \cdot mL^{-1}$, and similar Dh values were obtained when considering BSA buffer solutions at higher concentrations. A clear trend was observed for the dispersive effect by adsorbed proteins. However, the disagglomeration of P–SiO_2 was far from complete: a diameter of ca. 600 nm appears too large with respect to particle sizes observed by TEM.

For M–SiO_2 (Figure 4A, green symbols), these NPs appeared almost monodispersed in water because the measured Dh of ca. 50 nm is in good agreement with the main size observed by TEM (Figure 1, panels C,D). For these nanoparticles, electrostatic repulsive forces (ζ-potential = -29 mV) should prevail on attractive forces, and in particular on the hydrophobic ones, in agreement with the lower water contact angle measured (77.88 ± 2.06°) with respect to P-SiO_2. Similarly to the previous case, the suspension in PBS resulted in the formation of large agglomerates (Dh ca. 940 nm), which decrease in size when suspended in BSA solutions, more so for higher BSA concentration. For this type of NPs, the redispersion appeared more effective than for P–SiO_2, although incomplete (smallest Dh: ca. 125 nm). This behavior can be related to the larger hydrophylicity of M-SiO_2, then resulting in less extended hydrophobic interactions responsible for their agglomeration in PBS.

Besides quantitative differences, the dispersion effect of proteins towards agglomeration of both types of silica NPs deserves attention. The larger disruption of agglomerates attained by suspending them in BSA solutions at higher concentrations indicates that the process should depend on protein concentration gradients between outside and inside the agglomerates; i.e., it

should be driven by protein diffusion throughout inter-particle spaces. Moreover, the incomplete disagglomeration indicates that the protein diffusion did not reach the core of agglomerates. Hence, the systems finally obtained by adding the initial suspension of NPs in PBS to protein solutions at different concentrations can be described as suspensions of the parts of the agglomerates that resisted the disruption with proteins mainly adsorbed on their surface.

The same experimental conditions applied for DLS analysis of the suspension of NPs with irreversibly adsorbed proteins were also used for the ζ-potential measurements (Figure 4, panel B). When suspended in PBS buffer, both types of silica NPs exhibit negative ζ-potentials of –29 and –22 mV for P–SiO_2 and M–SiO_2, respectively, as expected from the deprotonation of surface silanols. Notably, the value obtained for M–SiO_2 is slightly less negative than for P–SiO_2, despite the significantly larger amount of silanols present in NPs prepared by microemulsion. This is in accordance with the overwhelming sub-surface location of Si–OH in these nanospheres, preventing their contribution to the interface with the aqueous medium.

In regard to protein molecules, BSA dissolved in PBS exhibited a ζ-potential of –9.5 mV in native form and–14.6 mV after denaturation by heating at 373 K for 10 min. In the case of P–SiO_2, the presence of irreversibly adsorbed proteins resulted in a significant increase of the ζ-potential from –29 to –17 mV (Δ = 12 mV) for samples in contact with protein solutions with BSA concentrations up to 1.0 $mg \cdot mL^{-1}$. When P–SiO_2 NPs were in contact with more concentrated BSA solutions (up to 7.5 $mg \cdot mL^{-1}$), a further slight increase of the ζ-potential from –17 to –13 mV was measured, and then the difference with respect to bare P–SiO_2 NPs increased to 16 mV.

Conversely, irreversibly adsorbed proteins shifted the ζ-potential of M–SiO_2 from −22 to ca. −20 mV when NPs were in contact with BSA solutions of up to 1 mg·mL^{-1} (panel B, green symbols). The potential then shifted to ca. −16 mV after incubation in the 2.5-mg·mL^{-1} BSA solution. Finally, slightly more negative ζ-potential values were measured for this type of NPs incubated in more concentrated BSA solutions. Hence, the maximum difference in ζ-potential between M–SiO_2 in the bare form and with irreversibly adsorbed BSA was only 6 mV.

The ζ-potential of M–SiO_2 with irreversibly adsorbed proteins also resulted in more negative values of a few mV than the corresponding P–SiO_2/BSA systems for BSA incubation solution concentrations of ≥ 1.0 mg·mL^{-1}. In particular, after incubation with the most concentrated BSA solution (7.5 mg·mL^{-1}), the ζ-potentials of P–SiO_2/BSA and M–SiO_2/BSA were −13 mV and −16 mV, respectively. The first value was between the ζ-potentials of native (–9.5 mV) and thermally treated (–15 mV) BSA molecules, with the latter being slightly less negative than that for P–SiO_2/BSA. Typically, the ζ-potential of a surface with adsorbed proteins is a combined function of coverage, orientation, and conformation of adsorbed proteins.[28] To obtain insights on the relative contribution of these factors, the amount of adsorbed proteins was measured for each incubation condition.

Amounts of BSA Adsorbed on SiO_2 NPs and Determination of Surface Coverage.

The total amounts of BSA adsorbed on the two types of SiO_2 NPs and related irreversible fractions are reported in Figure 5.

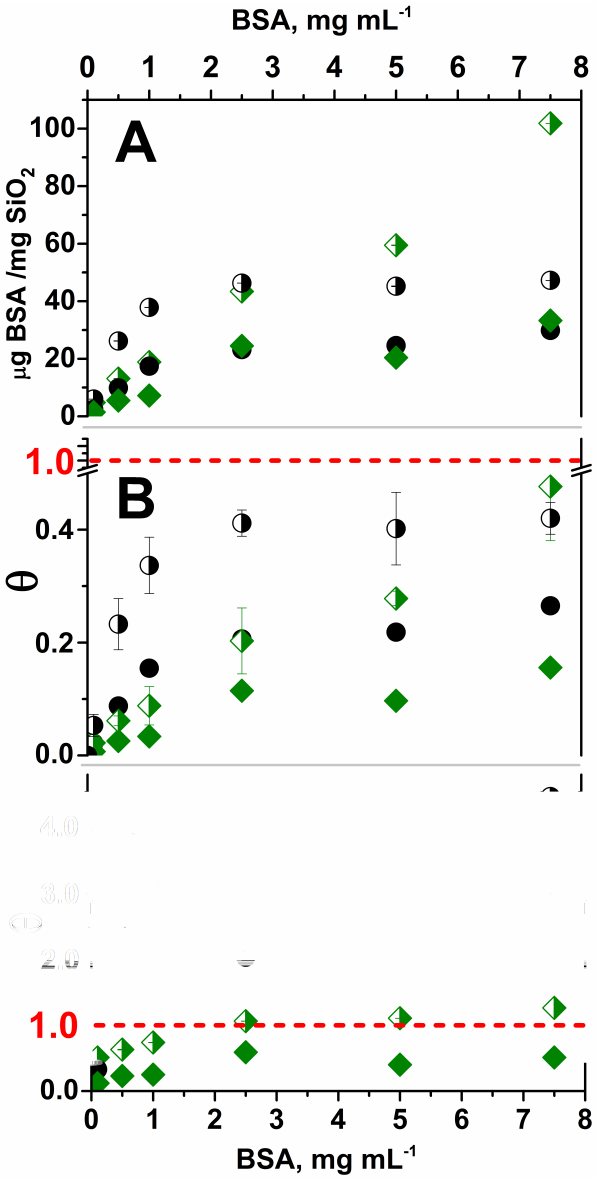

Figure 5. Amount of total (half symbols) and irreversibly (full symbols) BSA adsorbed on P–SiO_2 (black symbols) and M–SiO_2 (green symbols) per: A) mass of silica, B) theoretical monolayer (θ=1) calculated for BSA molecules adsorbed in a side-on way, and taking into consideration the specific surface area measured via N_2 adsorption (BET method), and C) theoretical monolayer (BSA molecules adsorbed in a side-on way) calculated taking into consideration the external specific surface area of NPs agglomerates observed by DLS. Note that in panels B and C the scale of the Y axis, where the coverage values are reported, is different.

The data in panel A are the mass of adsorbed protein per unit mass of silica. The total amount of BSA adsorbed on P–SiO_2 (half black symbols) gradually increases at an initial BSA concentration of 2.5 mg·mL^{-1} in the incubation solution and then remained constant. Conversely, the adsorption isotherm obtained for M–SiO_2 (half green symbols) increased monotonously up to the highest BSA concentration used (7.5 mg·mL^{-1}), reaching a final amount of adsorbed protein almost double that for P–SiO_2 and crossing the isotherm obtained for that material at a protein concentration of 2.5 mg·mL^{-1}. For the isotherms related to irreversibly adsorbed proteins (full symbols), data appeared more similar for the two materials and were significantly lower in both cases than the total amounts of adsorbed BSA.

The next step was evaluation of the surface coverage, which was initially carried out by considering the SSA_{BET} (Figure 5B). The main points resulting from this calculation are as follows: i) In all cases, the coverage remained well below the theoretical side-on monolayer (θ=1, corresponding to ca. 2250 μg BSA per m^2 of surface[16]), attaining a maximum value of ca. 0.5. ii) As a general trend, the coverage obtained for P–SiO_2 for both total and irreversibly adsorbed proteins was significantly higher than those corresponding for M–SiO_2, except for the highest coverage for total adsorbed proteins attained by incubation in protein solutions with a BSA concentration of 7.5 mg·mL^{-1}. At this concentration, the results were similar in both cases. The results obtained for P–SiO_2 were in agreement with previous studies.[28,50]

However, the DLS data indicated that protein adsorption should mainly occur on the external surface of the parts of initial agglomerates of both P–SiO_2 and M–SiO_2, which resisted the diffusion of proteins. Based on this, the surface coverage by BSA was recalculated while taking into account the estimated external surfaces of these agglomerates, which were modeled as

spheres with diameters equal to the measured Dh. Furthermore, the homogeneity of size and shape of M–SiO_2 NPs allowed for refinement of this model to some extent for evaluation of the silica mass present in the agglomerates made of these NPs. The homogeneity allowed for reliable calculation of the mass of each NP (with known density). In addition, these NPs were observed to pack in an hexagonal array.[37] The combination of these inputs resulted in better estimation of the SiO_2 mass present in the M–SiO_2 agglomerates and of their external specific surface area. The values and a description of the calculation procedure are reported in Table S1 in the SI.

Such a refinement was not possible for P–SiO_2 NPs, which exhibit a variety of sizes and shapes. Thus, the agglomerates of these NPs were considered as solid silica spheres, and the calculated specific surface area was underestimated. However, because the agglomerates were packed densely enough to prevent protein diffusion within inter-particle spaces, the assumption of agglomerates as solid spheres seems reasonable. The results of these calculations (Figure 5C; note that the scale along the Y axis is different from that in Figure 5B) indicate that protein multilayers should be present on the external surfaces of P–SiO_2 agglomerates for both the total (half black symbols) and irreversibly (full black symbols) adsorbed cases when starting incubations in protein solution with BSA concentrations of ≥0.5 and 1.0 $mg \cdot mL^{-1}$ (total and irreversible amounts, respectively). Conversely, total amounts of BSA adsorbed on M–SiO_2 attained the theoretical monolayer on the external surface of agglomerates incubated in the protein solutions with a BSA concentration 2.5 $mg \cdot mL^{-1}$ (half green symbols), while the coverage by irreversibly adsorbed proteins never exceed ca. 60% of the theoretical monolayer (full green symbols).

Notably, based on the proposed calculation of protein coverage, an irreversibly adsorbed

monolayer and a partial multilayer of proteins on P–SiO_2 NPs should have been attained by incubation in BSA solution with concentrations of 0.5 and 1.0 $mg \cdot mL^{-1}$, respectively (Figure 5C). The samples obtained in these incubation conditions also corresponded to the last two points, which were quite close to each other, of the first part of the trend exhibited by the ζ-potential of the P–SiO_2/BSA system depending on the BSA concentration in the incubation solutions (Figure 4B, black symbols). Most of the change with respect to bare NPs suspended in PBS occurred in these conditions (i.e., $\Delta\zeta$ = 12 mV for a total of 16 mV). This behavior is in agreement with the proposed complete coverage by proteins of the surface of agglomerates by incubation in those conditions. The subsequent minor changes in ζ-potential by further increasing the amount of adsorbed BSA might then be in agreement with the formation of thicker multilayers, exposing conformation and orientation that depend on the multilayer thickness at the surface proteins.

Unfortunately, the less negative ζ-potential of bare M–SiO_2 suspended in buffer prevented the possibility of unambiguously associating the smaller total change in ζ-potential obtained by BSA adsorption ($\Delta\zeta_{max}$= 6 mV; Figure 4B, green symbols) with the attainment of only sub-monolayer coverage indicated by the calculation. In fact, as a result of the less negative starting point and the smaller $\Delta\zeta$, most of the ζ-potential values obtained for the M–SiO_2/BSA systems appeared close to those measured for corresponding P–SiO_2/BSA systems. Additional insights on the actual possibility of the formation of a BSA multilayer or sub-monolayer on the surfaces on the P–SiO_2 and M–SiO_2 agglomerates were provided by spectroscopic investigations of adsorbed proteins.

CD-UV Spectra of Irreversibly Adsorbed Proteins

Figure 6 shows the CD–UV spectra of proteins irreversibly adsorbed on P–SiO_2 and M–SiO_2 (curves a-d in panels A and B, respectively). These were compared with the spectra of buffered solutions of BSA in the native form (blue curves) and after treatment at 373 K for 15 min (red curves).

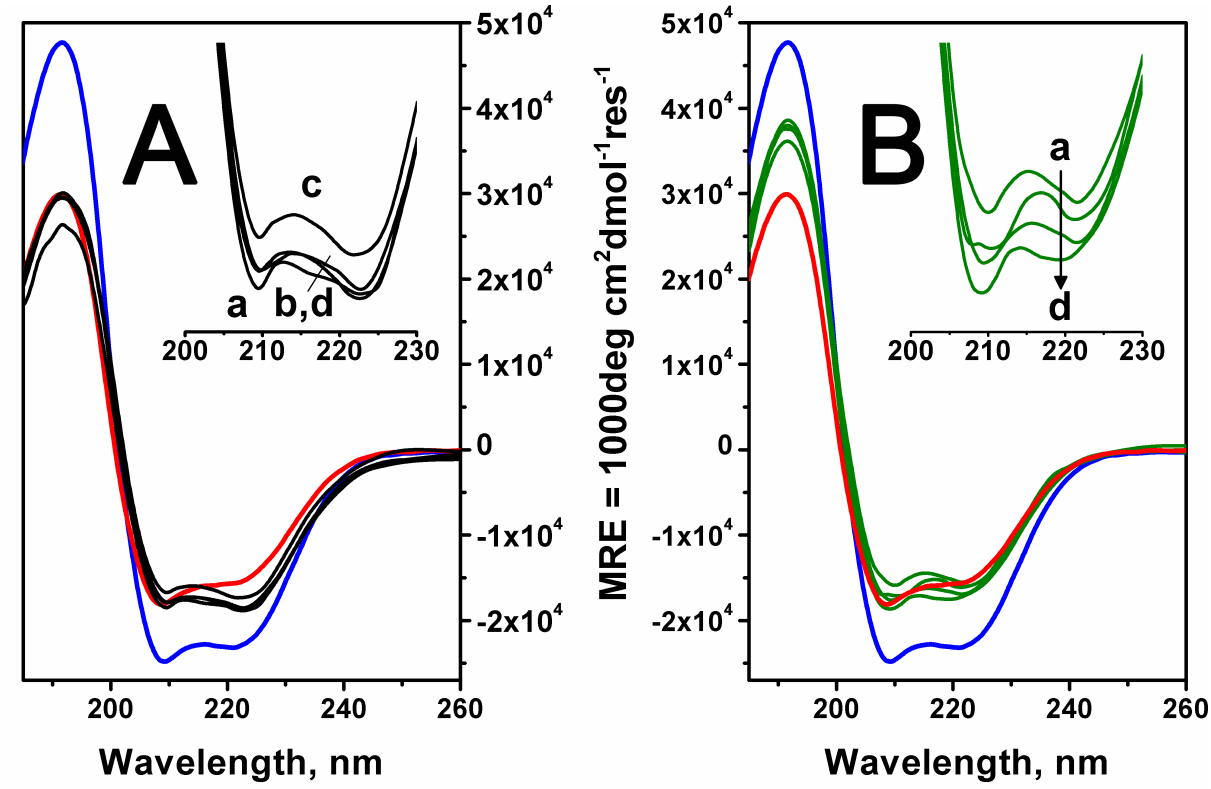

Figure 6. CD–UV spectra of BSA irreversibly adsorbed on P–SiO_2 (panel A, black curves) and M–SiO_2 (panel B, green curves) at different protein concentration in incubation solution: a) 0.5, b) 2.5, c) 5.0, d) 7.5 mg·mL^{-1}. Spectra are compared with those of solutions of BSA in native form (blue curves) and after thermal treatment at 373 K for 15 min (red curves). The intensity of the spectra was normalized with respect the protein content as described in Figure S4 in the SI.

Table 2. Values of the ratio between MRE at 208 and 222 nm (MRE_{208}/MRE_{222}) calculated for the CD-UV spectra of BSA in solution and adsorbed on the two types of SiO_2 NPs.

	MRE_{208}/MRE_{222} < 1	**MRE_{208}/MRE_{222} > 1**	
			BSA in solution
		1.012	native BSA
		1.015	heated at 373 K
adsorbed BSA			**adsorbed BSA**
spectrum a (P-SiO_2)	0.947	1.012	spectrum a (M-SiO_2)
spectrum b (P-SiO_2)	0.963	1.015	spectrum b (M-SiO_2)
spectrum c (P-SiO_2)	0.965	1.093	spectrum c (M-SiO_2)
spectrum d (P-SiO_2)	0.990	1.065	spectrum d (M-SiO_2)

The spectrum of native BSA exhibits the expected profile characterized by a positive signal at 192 nm (left-hand polarized $\pi_{nb} \rightarrow \pi^*$ electronic transition) and two negative components at 208 nm and 222 nm due to the right-hand polarized $\pi_{nb} \rightarrow \pi^*$ and $n \rightarrow \pi^*$ transitions, respectively.[51,52] The deconvolution of the spectral profile, carried out by CDNN software, resulted in a relative amount of α-helix, β-sheet, and unordered secondary motifs (Table 3, entry 1). Obtained data are consistent with literature ones[53] based on CDSSTR software based on CD spectra of proteins for which high-quality X-ray diffraction data are available.

After thermal treatment, the tree signals became less intense and exhibited changes in relative intensity, mainly as a consequence of significant conformational changes in favor of unordered secondary motifs (Table 3, entry 2), which is also in agreement with literature data,[54] where

deconvolution was carried out using UV-CD spectra poly-L-lysine with different secondary structure as reference.

Table 3. Results of the deconvolution of UV-CD spectra of BSA (water solutions, see Experimental section) in native forms and after heating for 15 min at 373 K, and irreversibly adsorbed on P–SiO_2 and M–SiO_2 at different protein concentration in incubation solution.

sample	BSA, $mg \cdot mL^{-1}$	α-helix (%)	β-sheet (%)	β-turn (%)	random coil (%)
BSA, solution		69 ± 3	9 ± 2	10 ± 0.5	12 ± 2
BSA, solution (treated at 373 K)		48 ± 2	10 ± 2	16 ± 1	27 ± 2
P–SiO_2	BSA, 0.5	37 ± 3	18 ± 1	16 ± 1	29 ± 2
	BSA, 2.5	37 ± 2	18 ± 1	15 ± 1	29 ± 1
	BSA, 5.0	36 ± 2	18 ± 2	16 ± 1	30 ± 1
	BSA, 7.5	36 ± 2	20 ± 2	16 ± 1	29 ± 1
M–SiO_2	BSA, 0.5	51 ± 2	10 ± 1	14 ± 1	25 ± 1
	BSA, 2.5	52 ± 4	11 ± 1	13 ± 0	24 ± 2
	BSA, 5.0	50 ± 3	11 ± 1	15 ± 0	25 ± 2
	BSA, 7.5	51 ± 4	11 ± 1	15 ± 1	24 ± 2

The spectra of irreversibly adsorbed proteins on the two types of SiO_2 NPs (curves a-d in both panels) normalized with respect to the same protein content (see Experimental section), generally appear closer to the spectrum of thermally treated BSA (red curves), showing the occurrence of conformational changes towards unordered secondary structures, as confirmed by deconvolution of spectra (Table 3, entries 3-10). However, an inversion of the relative intensity of the negative signals at ca. 208 and ca. 222 nm in favor of the second one occurred in the case of BSA on P–SiO_2 (Figure 6, inset of section A and Table 2). For the sake of clarity, the ratio between the MRE at these two positions was calculated for all spectra (MRE_{208}/MRE_{222}), and the results are reported in Table 2. For native and thermally treated proteins in solution, a ratio greater than one was obtained, which conversely became less than one for all BSA/P–SiO_2 samples. Similar behavior was observed for amyloid proteins adsorbed on Teflon particles.[54] This was a consequence of lateral interaction among adsorbed proteins at high surface coverage, thereby promoting intermolecular β-sheet formation. Hence, MRE_{208}/MRE_{222} values obtained for P–SiO_2/BSA samples are consistent with the presence of protein multilayers, which are proposed to form on the external surfaces of the agglomerates of these silica NPs where protein–protein interaction should occur. Accordingly, MRE_{208}/MRE_{222} values greater than one were calculated for BSA irreversibly adsorbed on M–SiO_2 (Figure 6, inset of section B and Table 2), attaining coverage that does not exceed the monolayer. The ensemble of data resulting from the deconvolution of CD–UV spectra of BSA in solution and adsorbed on the two types of silica appeared fully consistent with this (Table 3).

In the case of BSA in solution, by passing from the native form (entry 1) to the thermally treated one (entry 2), a decrease of the α-helix content in favor of β-turn and random coil

structural motifs (ca. +60% and +125%, respectively) occurred, while β-sheet secondary structures increased their relative content of ca. +15%. Basically, almost the same occurred for BSA on M–SiO_2 agglomerates (entries 7-10). Conversely, BSA on P–SiO_2 (entries 3-6) exhibited a decrease of the α-helix content in favor of not only β-turn and random coil structural motifs but also β-sheet structures. The relative amount of β-sheet structures almost doubled with respect to proteins in the native state (entry 1), which is in agreement with the expected protein–protein interaction occurring in a multilayered BSA hard corona.

The collection of data resulting from the calculation of protein surface coverage on the basis of the external surface of nanoparticle agglomerates and UV-CD measurements allows some comments on the origin of the formation of BSA sub-monolayer or multilayers irreversibly adsorbed toward dilution on the two types of silica NPs. The affinity of protein molecules for a sorbent surface affect the initial slope adsorption isotherms, i.e., higher the affinity, steeper the slope,[50] and on such a basis BSA exhibited a higher affinity towards P-SiO_2. When suspended in PBS (but the same occurred in water) these particles exhibited a more negative ζ-potential than M-SiO_2 (Figure 4B), the higher protein affinity towards P-SiO_2 has not an electrostatic origin, being BSA negatively charged at the pH of the incubation medium (see above). Conversely, P-SiO_2 appeared less hydrophilic than M-SiO_2 (Figure 4A and related comments) likely because of the different distribution of surface silanols, and hydrophobic interaction can promote protein adsorption.[56]

Noticeably, the formation of adsorbed multilayers can be related to the tendency of proteins to aggregate in solution, e.g. after conformational changes. However, this is not the case of thermally treated BSA, as indicated by the decrease of α-helix content, with respect to native

BSA, in favor of random coil, whereas the relative amount of β-sheet remained almost unchanged (see Table 3). It can be then proposed that the interaction of proteins with P-SiO_2 NPs agglomerates resulted in conformation of BSA molecules in contact with the surface promoting protein-protein interactions, against electrostatic repulsions among adsorbed proteins and the limited exposure of polar portions toward the aqueous medium. Likely, BSA in subsequently adsorbed layers could assume conformations resulting in a different balance among these factors, until the exposure of an outmost protein layer surface less active toward further irreversible adsorption, upon dilution, of BSA molecules.

CONCLUSION

The results indicated that the absorption of BSA on pyrolytic (P–SiO_2) and colloidal silica NPs (M–SiO_2 prepared by the inverse micelle microemulsion method) is a phenomenon where each component of the systems (proteins and SiO_2 NPs) has an effect on the other. In fact, BSA molecules act as a dispersing agent towards the large agglomerates formed by both types of NPs, which modify the conformation of adsorbed proteins. Notably, the distribution of silanols on the surface of the two types of silica NPs and, consequently, the surface hydrophobicity/hydrophylicity, appeared to affect the amount of adsorbed proteins significantly. The relative scarcity of isolated ≡Si–OH on M–SiO_2 can be indicated among the factors limiting the irreversible absorption of BSA with respect to P–SiO_2. Conversely, the surface ζ-potential of NPs might play a non-primary role in determining the amount of adsorbed proteins. M–SiO_2 NPs with less negative ζ-potential were found to adsorb less BSA than P–SiO_2 (independently of the

model used for the calculation of the coverage), despite the overall negative charge of these protein molecules in the incubation conditions.

From a methodological point of view, the persistence of the presence of NP agglomerates during the incubation in BSA solutions requires additional considerations of the surface area actually available to protein molecules when calculating the protein coverage. In this respect, the proposed model (which considers the external surface area of agglomerates with adsorbed protein molecules) produced data consistent with both the trend in ζ-potential for increasing amount of adsorbed proteins and CD-UV spectra (when applicable). These spectra provide evidence of protein–protein interaction for BSA on P–SiO_2, where the formation of multilayers of proteins irreversibly adsorbed toward dilution was proposed. A pictorial view of the main points commented on above is displayed in Scheme 1

Scheme 1. Graphical summary of the causal relationship among surface features of SiO_2 NPs, nanoparticles aggregation in PBS and protein coverage in BSA/PBS solution.

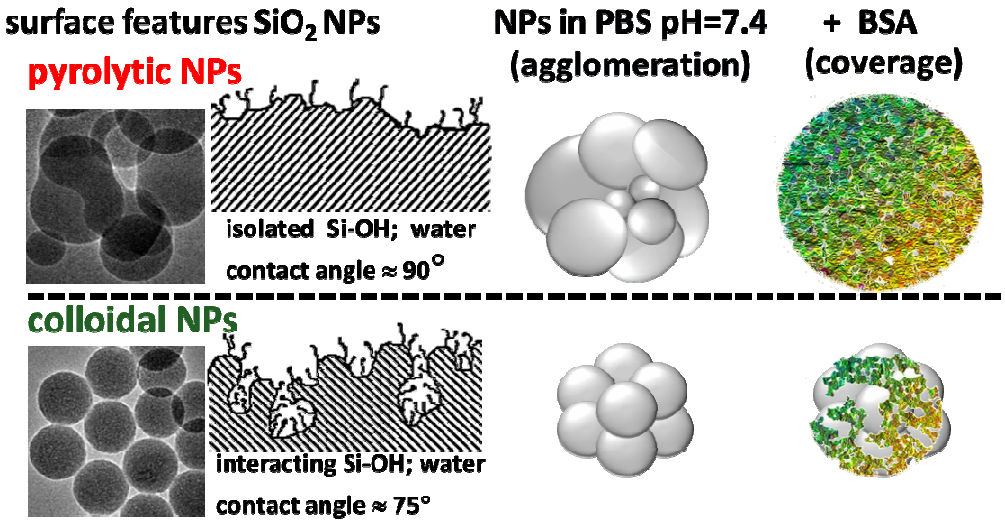

Finally, it can be considered that the investigation of the adsorption of BSA on NPs deals with a system that is much simpler than NPs in contact with plasma or serum (typically fetal bovine serum (FBS) or fetal calf serum (FCS)), which are usually considered for studying the formation of protein corona on colloidal silica NPs.[57,58]Albumin is the most abundant component of the protein pool in FBS and FCS, as well in human blood. In one study, it was also found to be the most abundant protein in the hard corona of silica NPs,[59] while in other cases, its content in the hard protein corona was very low.[60-62]

Physical parameters such as the surface curvature of NPs were proposed to play a role in the competitive adsorption of proteins in the process, resulting in the formation of the hard corona.[22] It could be of interest to investigate the possible contribution of different amounts and distributions of surface silanols to the composition of the hard protein corona on SiO_2 NPs. To the best of our knowledge, the formation of a protein corona on pyrolytic silica NPs has not been investigated yet. The results of such a study would be of interest for assessing whether the formation of BSA multilayers when these NPs are incubated with only this protein might correspond to its presence in a large amount in the protein corona formed by incubation in serum solutions.

ASSOCIATED CONTENT

Author Information

Corresponding Authors: *Gabriele Alberto, e-mail: gabriele.alberto@unito.it, telephone number +39-0116708385; ***Gianmario Martra,** e-mail: gianmario.martra@unito.it; telephone number: +39-0116706358;

Author Contributions

The manuscript was written through contributions of all authors. All authors have given approval to the final version of the manuscript.

Funding Sources

This research work received funding from EU (FP7 ILSES project, grant agreement n. 612620) and Fondazione CRT (call “Richieste ordinarie 2014”, project n. 2014.1041).

ACKNOWLEDGMENT

G.M. is obliged to Prof. Bice Fubini (University of Torino) for scientific collaboration and fruitful discussion on the interaction between inorganic materials and biomolecules since many years. Prof. P. Quagliotto (University of Torino) is acknowledged for the support for water contact angle measurements.

Supporting Information Description

Supporting Information Available: raw DLS data of: bare particles and proteins in buffer suspensions, NPs agglomerates in equilibrium with proteins after incubation, NPs incubated with BSA solutions, removed from the incubation media and resuspended in PBS buffer, i.e. carrying the irreversible fraction of adsorbed BSA; particle wetting curves ($mass^2$ vs time); IR spectra in controlled atmosphere of M–SiO_2 before and after contact with D_2O and tert-butanol; normalization method for the comparison between UV–CD spectra of BSA in solution and UV–CD spectra of proteins irreversibly adsorbed on P–SiO_2 and M–SiO_2. This material is available free of charge via the Internet at http://pubs.acs.org.

REFERENCES

[1] Fubini, B. Health Effect of Silica. In Legrand, A. P., Ed.; *The Surface Properties of Silicas*, John Wiley & Sons Chichester, UK, 1998.

[2] Hench, L. L.; Splinter, R. J.; Allen, W. C.; Greenlee, T. K. Bonding Mechanisms at the Interface of Ceramic Prosthetic Materials. *J. Biomed. Mater. Res. Symp.* **1971**, *2*, 117-141.

[3] Barbè, C.; Bartlett, J.; Kong, L.; Finnie, K.; Lin, H.Q.; Larkin, M.; Calleja, S.; Bush, A.; Calleja, G. Silica Particles: A Novel Drug-Delivery System. *Adv. Mater.* **2004**, *16*, 1959-1966.

[4] Piao, Y.; Burns, A.; Kim, J.; Wiesner, U.; Hyeon, T. Designed Fabrication of Silica-Based Nanostructured Particle Systems for Nanomedicine Applications. *Adv. Funct. Mater.* **2008**, *18*, 3745-3758.

[5] Vallet-Regi, M.; Balas, F.; Arcos, D. Mesoporous Materials for Drug Delivery. *Angew. Chem., Int. Ed.* **2007**, *46*, 7548-7558.

[6] Pasqua, L.; Cundari, S.; Ceresa, C.; Cavalletti, G. Recent Development, Applications, and Perspectives of Mesoporous Silica Particles in Medicine and Biotechnology. *Curr. Med. Chem.* **2009**, *16*, 3054-3063.

[7] Vivero-Escoto, J. L.; Slowing, I. I.; Trewyn, B. G.; Lin, V. S.-Y. Mesoporous Silica Nanoparticles for Intracellular Controlled Drug Delivery. *Small* **2010**, *6*, 1952-1967.

[8] Tang, L.; Cheng, J.; Nonporous Silica Nanoparticles for Nanomedicine Application. *Nano*

Today. **2013**, *8*, 290-312.

[9] Walczyk, D.; Bombelli, F. B.; Monopoli, M. P.; Lynch, I.; Dawson, K. A. What the Cell "Sees" in Bionanoscience. *J. Am. Chem. Soc.*, **2010**, *132*, 5761-5768.

[10] Mahmoudi, M.; Lynch, I.; Ejtehadi, M. R.; Monopoli, M. P.; Bombelli, F. B.; Laurent S. Protein-nanoparticle Interactions: Opportunities and Challenges. *Chem. Rev.* **2011**, *111*, 5610-5637.

[11] Hamad-Schifferli, K. How Can We Exploit the Protein Corona? *Nanomedicine*, **2013**, *8*, 1-3.

[12] Kasemo, B. Biological Surface Science. *Surf. Sci.* **2002**, *500*, 656-677.

[13] Serpooshan, V.; Mahmoudi, M.; Zhao, M.; Wei, K.; Sivanesan, S.; Motamedchaboki, K.; Malkovskiy, A. V.; Goldstone, A. B.; Cohen, J. E.; Yang, P. C.; Rajadas, J. Protein Corona Influences Cell–Biomaterial Interactions in Nanostructured Tissue Engineering Scaffolds. *Adv. Funct. Mater.* **2015**, *25*, 4379-4389.

[14] Norde, W.; Favier, J. P. Structure of Adsorbed and Desorbed Proteins. *Colloid Surface***. 1992**, *64*, 87-93.

[15] Orts-Gil, G.; Natte, K.; Drescher, D.; Bresch, H.; Mantion, A.; Kneipp, J.; Österle, W. Characterization of Silica Nanoparticles Prior to In Vitro Studies: from Primary Particles to Agglomerates. *J. Nanopart. Res.* **2011**, *13*, 1593-1604.

[16] Rezwan, K.; Meier, L. P.; Rezwan, M.; Vörös, J.; Textor, M.; Gauckler, L. J. Bovine

Serum Albumin Adsorption onto Colloidal Al_2O_3 Particles: A new Model Based on Zeta Potential and UV-Vis Measurements. *Langmuir* **2004**, *20*, 10055-10061.

[17] Kittler, S.; Greulich, C.; Gebauer, J. S.; Diendorf, J.; Treuel, L.; Ruiz, L.; Gonzalez-Calbet, J. M.; Vallet-Regi, M.; Zellner, R.; Köller, M.; Epple, M. The Influence of Proteins on the Dispersability and Cell-Biological Activity of Silver Nanoparticles. *J. Mater. Chem.* **2010**, *20*, 512-518.

[18] Liu, W.; Rose, J.; Plantevin, S.; Auffan, M.; Bottero, J.-Y.; Vidaud, C. Protein Corona Formation for Nanomaterials and Proteins of a Similar Size: Hard or Soft Corona? *Nanoscale* **2013**, *5*, 1658-1668.

[19] Peters, T. *All About Albumin*; Academic Press: San Diego, US, 1995.

[20] Nakanishi, K.; Sakiyama, T.; Imamura, K. On the Adsorption of Proteins on Solid Surfaces, a Common but Very Complicated Phenomenon. *J. Biosci. Bioeng.* **2001**, *91*, 233-244.

[21] Rabe, M.; Verdes, D.; Seeger, S. Understanding Protein Adsorption Phenomena at Solid Surfaces. *Adv. Colloid Interface Sci.* **2011**, *162*, 87-106.

[22] Lundqvist, M.; Sethson, I.; Jonsson, B.-H. Protein Adsorption onto Silica Nanoparticles: Conformational Changes Depend on the Particles' Curvature and the Protein Stability. *Langmuir*, **2004**, *20*, 10639-10647.

[23] Wang, J.; Jensen, U. B.; Jensen, G. V.; Shipovskov, S.; Balakrishnan, V. S.; Otzen, D.; Pedersen, J.S.; Besenbacher, F.; Sutherland, D. S. Soft Interactions at Nanoparticles Alter

Protein Function and Conformation in a Size Dependent Manner. *Nano Lett.* **2011**, *11*, 4985-4991.

[24] Orts-Gil, G.; Natte, K.; Thiermann, R.; Girod, M.; Rades, S.; Kalbe, H.; Thünemann A. F.; Maskos, M.; Österle, W. On the Role of Surface Composition and Curvature on Biointerface Formation and Colloidal Stability of Nanoparticles in a Protein-Rich Model System. *Colloid Surface B* **2013**, *108*, 110-119.

[25] Shen, S.-C.; Ng, W. K.; Chia, L.; Dong, Y.-C.; Tan, R. B. H. Sonochemical Synthesis of (3-amminopropyl)triethoxysilane-modified Monodispersed Silica Nanoparticles for Protein Immobilization. *Mater. Res. Bull.* **2011,** *46*, 1665-1669.

[26] Tenzer, S.; Docter, D.; Kuharev, J.; Musyanovych, A.; Fetz, V.; Hecht, R.; Schlenk, F.; Fischer, D.; Kiouptsi, K.; Reinhardt, C. et al. Rapid Formation of Plasma Protein Corona Critically Affects Nanoparticle Pathophysiology. *Nat. Nanotechnol.* **2013,** *8*, 772–781.

[27] Mironyuk, I. F.; Gunko, V. M., Turov, V. V.; Zarko, V. I.; Leboda, R.; Skubiszewska-Zięba, J. Characterization of Fumed Silicas and their Interaction with Water and Dissolved Proteins. *Colloid Surface A* **2001**, *180*, 8336-8346.

[28] Turci, F.; Colonna, M.; Boscolo, B.; Fenoglio, I.; Fubini, B. An Integrated Approach to the Study of the Interaction Between Proteins and Nanoparticles. *Langmuir* **2010**, *26*, 8336-8346.

[29] Marucco, A.; Turci, F.; O'Neill, L.; Byrne, H. J.; Fubini, B.; Fenoglio, I. Hydroxyl Density Affects the Interaction of Fibrinogen with Silica Nanoparticles at Physiological

Concentration. *J. Colloid. Interf. Sci*. **2014**, *419*, 86-94.

[30] Bolis, V.; Fubini, B.; Marchese, L.; Martra, G.; Costa, D. Hydrophilic and Hydrophobic sites on Dehydrated Crystalline and Amorphous Silicas. *J. Chem. Soc. Faraday Trans.* **1991**, *87*, 497-505.

[31] Zhang, H.; Dunphy, D. R.; Jiang, X.; Meng, H.; Sun, B.; Tarn, D.; Xue, M.; Wang, X.; Lin, S.; Ji, Z.; Li, R.; Garcia, F. L.; Yang, J.; Kirk, M. L.; Xia, T.; Zink, J. I.; Nel, A.; Brinker, J. Processing Pathway Dependence of Amorphous Silica Nanoparticle Toxicity: Colloidal vs Pyrolytic. *J. Am. Chem. Soc.* **2012**, *134*, 15790-15804.

[32] Stöber, W.; Fink, A.; Bohn, E. Controlled Growth of Monodisperse Silica Spheres in the Micron Size Range. *J. Colloid. Interf. Sci*. **1968**, *26*, 62-69.

[33] Van Helden, A. K.; Jansen, J. W.; Vrij, A. Preparation and Characterization of Spherical Monodisperse Silica Dispersions in Nonaqueous Solvents. *J. Colloid. Interf. Sci*. **1981**, *81*, 354-368.

[34] Szekeres, M.; Tóth, J.; Dékány, I. Specific Surface Area of Stoeber Silica Determined by Various Experimental Methods *Langmuir* **2002**, *18*, 2678-2685.

[35] Burneau, A.; Barrès, O.; Gallas, J.P.; Lavalley, J.C. Comparative Study of the Surface Hydroxyl Groups of Fumed and Precipitated Silicas. 2. Characterization by Infrared Spectroscopy of the Interactions with Water. *Langmuir* **1990**, *6*, 1364-1372.

[36] Del Pino, P.; Pelaz, B.; Zhang, Q.; Maffre, P.; Nienhaus, G. U.; Parak, W. J. Protein Corona Formation Around Nanoparticles – From the Past to the Future. *Mater. Horiz.*

2013, *1*, 301-313.

[37] Alberto, G.; Miletto, I.; Viscardi, G.; Caputo, G.; Latterini, L.; Coluccia, S.; Martra, G. Hybrid Cyanine-Silica Nanoparticles: Homogeneous Photoemission Behavior of Entrapped Fluorophores and Consequent High Brightness Enhancement. *J. Phys. Chem. C* **2009**, *113*, 21048-21053.

[38] Miletto, I.; Gilardino, A.; Zamburlin, P.; Dalmazzo, S.; Lovisolo, D.; Caputo, G.; Viscardi, G.; Martra, G. Highly Bright and Photostable Cyanine Dye-Doped Silica Nanoparticles for Optical Imaging: Photophysical Characterization and Cell Tests. *Dyes Pigments* **2010**, *84*, 121-127.

[39] Burneau, A. E.; Gallas, J. P. Vibrational Spectroscopies—Hydroxyl groups on silica surfaces. In *The Surface Properties of Silicas*; Legrand, A.P. Ed.; John Wiley: Chichester, UK, 1998.

[40] Neirinck, B.; van Deursen, J.; van der Biest, O.; Vleugels, J. Wettability Assessment of Submicrometer Alumina Powder Using a Modified Washburn Method. *J. Am. Ceram. Soc.*, **2010**, *93*, 2515-2518.

[41] Ugliengo, P.; Sodupe, M.; Nusso, F.; Bush, I. J.; Orlando, R.; Dovesi, R. Realistic Models of Hydroxylated Amorphous Silica Surfaces and MCM-41 Mesoporous Material Simulated by Large-scale Periodic B3LYP Calculations. *Adv. Mater.* **2008**, *20,* 4579-4583.

[42] Takeuchi, M.; Bertinetti, L.; Martra, G.; Coluccia, S.; Anpo, M. States of H_2O Adsorbed

on Oxides: An Investigation by Near and Mid Infrared Spectroscopy. *Appl. Catal. A-Gen.* **2006**, *307*, 13-20.

[43] Rice, G. L.; Scott, S. L. Characterization of Silica-Supported Vanadium(V) Complexes Derived from Molecular Precursors and Their Ligand Exchange Reactions. *Langmuir* **1997**, *13*, 1545-1551.

[44] Deguns, E. W.; Taha, Z.; Meitzner, G. D. Scott, S. L. An X-ray Absorption Study of Two $VOCl_3$-Modified Silicas: Evidence for Chloride-Silica Interactions. *J. Phys. Chem. B* **2005**, *109*, 5005-5011.

[45] Makarova, M. A.; Ojo, A. F.; Karim, K.; Hunger, M.; Dwyer, J. FTIR Study of Weak Hydrogen Bonding of Brönsted Hydroxyls in Zeolites and Aluminophosphates *J. Phys. Chem.* **1994**, *98*, 3619-3623.

[46] Carteret, C. Mid- and Near-Infrared Study of Hydroxyl Groups at a Silica Surface: H-Bond Effect. *J. Phys. Chem. C* **2009**, *113*, 13300-13308.

[47] Israelachvili, J. *Intermolecular and Surface Forces*, Academic Press, London, UK, second edition, 1991.

[48] Kulkarni, S. A.; Ogale, S. B.; Vijayamohanan, K. P. Tuning the Hydrophobic Properties of Silica Particles by Surface Silanization Using Mixed Self-assembled Monolayers. *J. Colloid. Interf. Sci*. **2007**, *318*, 372-379.

[49] Texter, J.; Klier, K.; Zettlemoyer, A.C. Water at Surfaces. *Prog. Surf. Membrane Sci.* **1978**, *12*, 327-403.

[50] Norde, W.; Giacomelli, C. E. BSA Structural Changes During Homomolecular Exchange Between the Adsorbed and the Dissolved States *J. Biotechnol*. **2000**, *79*, 259-268.

[51] Moffit, W. The Optical Rotatory Dispersion of Simple Polypeptides. II. *P. Natl. Acad. Sci. USA* **1956**, *42*, 736-746.

[52] Beychok, S. Circular Dichroism of Biological Macromolecules. *Science* **1966**, *154*, 1288-1299.

[53] Charbonneau, D. M.; Tajmir-Riahi, H. Study of the Interaction of Cationic Lipids with Bovine Serum Albumin. *J. Phys. Chem. B* **2010**, *114*, 1148–1155.

[54] Giacomelli, C.; Norde, W. The Adsorption–Desorption Cycle. Reversibility of the BSA–Silica System. *J. Colloid. Interf. Sci.* **2001**, *233*, 234-240.

[55] Giacomelli, C.; Norde, W. Influence of Hydrophobic Teflon Particles on the Structure of Amyloid B-Peptide. *Biomacromolecules* **2003**, *4*, 1719-1726.

[56] Norde, W. Driving Forces for Protein Adsorption at Solid Surfaces. *Macromol. Symp.* **1996**, *103*, 5-18.

[57] Lesniak, A.; Fenaroli, F.; Monopoli, M. P.; Åberg, C.; Dawson, K. A.; Salvati, A. Effects of the Presence or Absence of a Protein Corona on Silica Nanoparticle Uptake and Impact on Cells. *ACS Nano* **2012**, *6*, 5845-5857.

[58] Díaz, B.; Sánchez-Espinel, C.; Arruebo, M.; Faro, J.; de Miguel, E.; Magadán, S.; Yague, C.; Fernandez-Pacheco, R.; Ibarra, M. R.; Santamaria, J.; González-Fernández, A.

Assessing Methods for Blood Cell Cytotoxic Responses to Inorganic Nanoparticles and Nanoparticle Aggregates. *Small* **2008**, *4*, 2025–2034.

[59] Tenzer, S.; Docter, D.; Rosfa, S.; Wlodarski, A.; Kuharev, J.; Rekik, A.; Knauer, S. K.; Bantz, C., Nawroth, T.; Bier, C.; et al. Nanoparticle Size Is a Critical Physicochemical Determinant of the Human Blood Plasma Corona: A Comprehensive Quantitative Proteomic Analysis. *ACS Nano* **2011**, *5*, 7155–7167.

[60] Cedervall, T.; Lynch, I.; Lindman, S.; Berggård, T.; Thulin, E.; Nilsson, H.; Dawson, K. A.; Linse, S. Understanding the Nanoparticle–Protein Corona Using Methods to Quantify Exchange Rates and Affinities of Proteins for Nanoparticles. *PNAS* **2007**, *104*, 2050-2055.

[61] Dutta, D.; Sundaram, S. K.; Teeguarden, J. G.; Riley, B. J.; Fifield, L. S., Jacobs, J. M.; Addleman, S. R.; Kaysen, G. A.; Moudgil, B. M.; Weber, T. J. Adsorbed Proteins Influence the Biological Activity and Molecular Targeting of Nanomaterials. *Toxicol, Sci.* **2007**, *100*, 303-315.

[62] Lundqvist, M.; Stigler, J.; Cedervall, T.; Berggård, T.; Flanagan, M.B.; Lynch, I.; Elia, G.; Dawson, K. The Evolution of the Protein Corona around Nanoparticles: A Test Study. *ACS Nano* **2011**, *5*, 7503-7509.